UNIVERSITY OF CALIFORNIA,
IRVINE

Concentration Dependent Depth Distribution of Acetonitrile at the Liquid/Vapor Interface of Aqueous Solutions

DISSERTATION

submitted in partial satisfaction of the requirements
for the degree of

MASTER OF SCIENCE

in Chemistry,
Chemical and Materials Physics

by

Michael J. Makowski

Thesis Committee:
Professor John C. Hemminger, Chair
Professor Douglas J. Tobias
Professor Wilson Ho

2016

DEDICATION

To

my wife, Brittany, and my two boys, Michael and Zachary, as they are my compass.

For their continued support, despite having to endure many absent hours, late nights and unavoidable frustrations accompanying the demands of research, I dedicate this work to them.

TABLE OF CONTENTS

LIST OF FIGURES

LIST OF TABLES

ACKNOWLEDGMENTS

Great thanks and appreciation must go to Professor John C. Hemminger for advising with an open mind, allowing my thoughts to influence our research at greater lengths than I could ever request. To learn from the best has been no less humbling than it has been an honor. For this opportunity, I thank you.

I must also express sincere gratitude to Dr. Abe Stern and Professor Doug Tobias for introducing me to, and teaching me the ways of computational science. Additional thanks goes to Professor Wilson Ho for the continued inspiration.

This work was supported by the National Science Foundation Grant No. CHE 0909227 and the AirUCI program at the University of California, Irvine. The Advanced Light Source is supported by the Office of Science, Office of Basic Energy Sciences

ABSTRACT OF THE THESIS

Concentration Dependent Depth Distribution of Acetonitrile at the Liquid/Vapor Interface of Aqueous Solutions

By

Michael J. Makowski

Master of Science in Chemistry,
Chemical and Materials Physics

University of California, Irvine, 2016

Professor John C. Hemminger, Chair

Chemical reactions occur ubiquitously at the air/water interfaces of oceans and rivers, as well as on aerosols in the atmosphere. Presently, these occurrences are not well understood. In recent years, however, this field has drawn a wave of interest, due to the emergence of experimental techniques sensitive to the liquid surface and more powerful computing architectures that permit the simulations of large systems. The importance of understanding molecular transfer through the liquid/vapor interface to better interpret atmospheric chemical processes cannot be overstated. Reported here, are molecular dynamics simulations of acetonitrile-water binary solutions at concentrations of 0.05–0.6 mole fraction. Evaluating systems of low bulk acetonitrile concentration reveals an enhanced population of the solute near the liquid/vapor interface. These surface-bound acetonitrile molecules exhibit a specific preferential anisotropy, where temporally averaged probability distributions of molecular orientation have indicated interfacial acetonitrile laying nearly flat along the surface with the terminal methyl group directed away from the condensed phase. Upon increasing the bulk concentration, the formation of acetonitrile domains are promoted by interactions between hydrophobic methyl moieties. Dipole-dipole interactions facilitate a pseudonematic, antiparallel pairing of near-neighbor molecules, a

behavior present in both bulk solution and near the liquid/vapor interface. In the latter, the preferred orientation of acetonitrile flattens further to accommodate antiparallel pairing of neighbor molecules, such that the methyl group remains above the solution, protected from unfavorable hydration. This study offers an interpretation of a binary liquid solution that manifests behavior similar to liquid-crystals through preferred orientations and pseudonematic antiparallel pairing.

Chapter 1

Introduction

Acetonitrile (MeCN), or CH_3CN, is water-miscible and has a high dielectric constant.[1] It has therefore found routine use in the laboratory as a common solvent for HPLC and other techniques. In the environment, MeCN maintains a considerable atmospheric presence that is sourced predominantly through emissions of biomass burning.[2, 3] While acetonitrile undergoes oceanic uptake in the troposphere[4] and photodissociation driven interactions with hydroxyl radicals in the stratosphere, its atmospheric residence time may fall anywhere between two weeks and three years.[5] Accordingly, constructing a meaningful interpretation of the intermolecular interactions between water and MeCN is clearly motivated by its presence in both the laboratory and environmental settings.

It is not surprising that bulk solvation of acetonitrile in water has been heavily scrutinized over the past few decades, involving discussions of "microheterogenity", or nonhomogeneous molecular solvation.[6] Raman scattering studies have evidenced this behavior through distinct signatures corresponding to either hydrated or bulk-like liquid MeCN,[7] while IR Spectroscopy measurements have suggested a preferential solvation that leads to the clustering of like-molecules over an extensive range of MeCN

compositions.[8, 9, 10] A series of experimental studies by Takamuku *et al.* have confirmed this microheterogenity and further suggested an antiparallel ordering between MeCN pairs in the bulk-like domains.[11, 12, 13] Not limited to experimentation alone, Molecular Dynamics (MD) simulations[14] and Monte Carlo studies[15] have demonstrated an absence of favorable hydration of the methyl group, while the experimental detection of microheterogenteity was corroborated through MD simulations by Mountain.[16, 17]

Given the environmental relevance of MeCN uptake in water, as well as the introduction of experimental techniques capable of probing the liquid surface, recent studies have begun targeting MeCN solvation at the aqueous/vapor interface. Zhang *et al.*, for example, have used sum frequency generation (SFG) to investigate nonrandom orientation at the solution surface and found a preferential alignment of 40° off normal for concentrations less than 0.07 mole fraction (mf).[18, 19] Above this concentration, they observed an abrupt shift toward flatter laying molecules at 70°, justified as being due to the loss of hydrogen bonding with water in favor of dipole-dipole interactions with adjacent MeCN as the surface population rises.[20] Kim *et al.* arrived at a slightly different result of 23° or less with bulk acetonitrile concentrations at or below 0.2 mf.[21] They have, however, also predicted further tilting at higher concentrations. Yet one other SFG study proposed a mix of upward and downward facing MeCN molecules at the surface,[22] further dividing any knowledgeable consensus of interfacial orientation via experimental observation.

Using MD simulations, Paul and Chandra reported surface-bound MeCN perpendicular to the surface at all compositions with no indication of reconstruction,[23] while an alternative computational report has detected dipoles that are parallel to the surface.[24] In a detailed analysis of the corrugated liquid surface, Pártay *et al.* have found MeCN either laying 20° with respect to the surface plane (nearly parallel) when at the crest of a capillary wave, or perpendicular to the surface if found within a well.[25] Ultimately, they concluded that

acetonitrile forms a layered array at the liquid/vapor interface where the first sublayer aligns antiparallel to that of the topmost layer.

Notwithstanding the existing controversy over the angular distribution of MeCN at the aqueous/vapor interface, the enhanced surface presence of MeCN at low bulk concentration is now largely accepted. Principally motivating our study is a particularly recent Liquid-Jet Ambient Pressure X-ray Photoelectron Spectroscopy (LJ-APXPS) experiment quantifying the surface adsorption of acetonitrile at the liquid/vapor interface of aqueous solutions.[26] Here, they identified the existence of a dipole layer formed at the interface due to the net alignment of the surface-bound acetonitrile and have discovered a saturation of the MeCN surface enhancement at an approximate bulk concentration of 0.2 mf, coincidentally also corroborating concentration-dependent vapor pressure measurements from a few decades prior.[27]

The objective of this report is to remedy the disparity in the literature concerning the interfacial angular distribution, as well as to correlate the influence of microheterogeneity to the preferred anisotropy at the surface. It is believed that over a moderate range of acetonitrile compositions, local inhomogeneities often described as bulk behavior will mar the ordered alignment of previously uncoupled solute molecules at the surface as the packing density increases. These concepts will be considered in the text to follow.

Chapter 2

Computational Background

Molecular dynamics (MD) is a method of numerically integrating the equations of motion to derive positions and momenta of all particles in a system. Sampling the phase space of the system over a length of time, sufficient to capture a significant number of available microstates, the number ultimately dependent on the complexity of the system, allows for the measurement of ensemble averages as well as dynamical information.[28] The resulting "trajectories" may also be used to visualize the system over the course of the simulation. These aspects of MD make the technique very attractive for understanding atomic and molecular behavior. Moreover, with the continued growth of increasingly powerful computer architecture, the study of large and highly complex molecular systems is of greater practicality now than over the last few decades.

Generating these trajectories requires a numeric integrator. One common integrator for computing positions and velocities over discrete time steps is the velocity-Verlet[29] algorithm, based on the original Verlet algorithm[30] which, unlike the former, does not provide the ability to dynamically integrate velocities. The velocity-Verlet method employs

the following system of equations:[28, 29]

$$r_i(t + \Delta t) = r_i(t) + \Delta t \mathbf{v}_i(t) + \frac{\Delta t^2}{2m_i}\mathbf{F}_i(t), \tag{2.1}$$

$$v_i(t + \Delta t) = v_i(t) + \frac{\Delta t}{2m_i}(\mathbf{F}_i(t) + \mathbf{F}_i(t + \Delta t)), \tag{2.2}$$

such that with knowledge of the current position and velocity, those for the following step may be computed.

Attempting to accurately model a realistic system of molecules relies on properly addressing the forces incurred by each atom, a task often not trivial. In condensed matter systems, one is concerned with both intramolecular and intermolecular interaction potentials. The former, describing bonding interactions, includes the following:[31]

$$E_b = \sum k_b(r - r_0)^2, \tag{2.3}$$

$$E_\theta = \sum k_\theta(\theta - \theta_0)^2, \tag{2.4}$$

$$E_\phi = \sum |k_\phi| - k_\phi cos(n\phi) \qquad n = 1, 2, 3, 4, 5, 6 \tag{2.5}$$

where E_b is the interaction potential corresponding to bond stretching, E_θ of bond bending and E_ϕ of proper dihedral torsions. Required for computation are the respective force constants (i.e. k^b, k^θ and k^ϕ), equilibrium values (i.e. r_0 and θ_0) and multiplicity, n, describing the number of torsional energy minima.

Intermolecular interaction potentials include the Lennard-Jones potential,[32]

$$E_{LJ}(r) = \sum_i \sum_j 4\epsilon((\frac{\sigma}{r_{ij}})^{12} - (\frac{\sigma}{r_{ij}})^6), \tag{2.6}$$

that contains ϵ and σ as the potential well depth and equilibrium radius, respectively. This describes the van der Waals forces experienced by neighboring nonbonded atoms separated

by r_{ij}. Along with the Coulombic potential,

$$E_C = \sum_i \sum_j \frac{q_i q_j}{4\pi\epsilon_0 r_{ij}}, \tag{2.7}$$

these long range interactions (i.e. on the scale of many molecule lengths) make up the primary contribution to an increased computational expense of simulating progressively larger systems. This is especially true when implementing periodic boundary conditions, where the system is replicated indefinitely beyond the original simulation cell. One way to counter this is in using what is known as the miminum image convention.[33] Here, molecules will only interact with others that lay within a radius defined by the dimensions of the original cell. Therefore, calculation of the Lennard-Jones potential may be truncated by a spherical cutoff, which may either be done abruptly or with a smooth asymptotic truncation to reduce the deviation from a nontruncted calculation.

Computing the Coulombic contribution to the total interaction potential involved in the integrator may actually be done without a truncation. These "full-range" electrostatic calculations are performed with a method known as the smooth particle mesh Ewald (PME) summation, with a computation cost on the order of $N\ log(N)$, (with N being the number of interaction sites), and in the forms:[34]

$$E_{dir} = \frac{1}{2} \sum_n \sum_{i,j=1}^{N} \frac{q_i q_j\ erfc(\beta|\mathbf{r}_j - \mathbf{r}_i + \mathbf{n}|)}{|\mathbf{r}_j - \mathbf{r}_i + \mathbf{n}|}, \tag{2.8}$$

$$E_{rec} = \frac{1}{2\pi V} \sum_{m \neq 0} \frac{exp(-\pi^2 \mathbf{m}^2/\beta^2)}{\mathbf{m}^2} S(\mathbf{m}) S(-\mathbf{m}), \tag{2.9}$$

$$E_{cor} = -\frac{1}{2} \sum_{(i,j) \in M} \frac{q_i q_j\ erf(\beta|\mathbf{r}_i - \mathbf{r}_j|)}{|\mathbf{r}_i - \mathbf{r}_j|} - \frac{\beta}{\sqrt{\pi}} \sum_{i=1}^{N} q_i^2. \tag{2.10}$$

These three, respectively declared as direct, reciprocal and correction terms, sum to form the total electrostatic energy contribution to the total interaction potential.

Choosing the correct parameter set for the potentials between atom pairs is the most important aspect of beginning of a Molecular Dynamics simulation. Incorrectly defining equilibrium constants, for example, may result in a successful simulation, but not a realistic or accurate one. However, once the system has been properly parameterized, it is only left to describe the constraints to be placed and observables of interest to probe.

Simulations in the following discussion involve constraining pressure and temperature, as in the isothermal-isobaric ensemble (NPT), as well as volume and temperature, as in the canonical ensemble (NVT). The simulation package, NAMD,[35] provides the tools necessary to accomplish this, by parallelizing the essential formulas to permit the rapid computation of the velocity-Verlet integrator with all potentials and perturbations (e.g. temperature and pressure) included. Upon acquisition of the completed trajectories, intermolecular radial and orientational correlations were studied between molecules of acetonitrile and water within liquid solutions. This is to be presented in the following chapters.

Chapter 3

Details of Simulation

Molecular Dynamics simulations described here were calculated with the parallel computing package, NAMD.[35] The resulting trajectories have been graphically modeled with VMD.[36] Each system contained a total of 1728 molecules with nominal concentrations between 0.05–0.6 mf (see Table 3.1 for absolute bulk concentrations). Liquid slabs of finite thickness were formed during equilibration, such that a region of bulk solution is bounded by two non-interacting liquid/vapor interfaces. The slabs were confined to a $3.8 \times 3.8 \times 14\ nm^3$ box with three dimensional periodic boundary conditions, where the surface normal is directed along the long axis.

Equilibration and a 10 ns simulation for analysis were performed in the isothermal-isobaric and canonical ensembles, respectively. Pressures were coupled with a Berendsen pressure bath and Langevin dynamics provided stochastic temperature control about a mean of 300 K. The multistep integrator of NAMD permitted the calculation of bonded interactions every 1 fs, nonbonded interactions every 2 fs and full range electrostatics every 4 fs. Here, a 12 Å smooth cutoff was applied to nonbonded Lennard-Jones interactions and the smooth mesh Ewald Summation was implemented for electrostatics.[34]

Table 3.1: Slab concentrations

No. of H_2O molecules	No. of MeCN molecules	Nominal conc. (mf)	Absolute Bulk conc. (mf)
1642	86	0.05	0.032
1607	121	0.07	0.045
1555	173	0.1	0.074
1382	346	0.2	0.17
1210	518	0.3	0.27
1037	619	0.4	0.38
864	864	0.5	0.48
619	1037	0.6	0.59

Table 3.2: Potential parameters of acetonitrile[37] and TIP3P[38] Water

Site	ϵ (kcal mol^{-1})	σ (Å)	q (charge)
N_{CN}	0.17	1.824	-0.5126
C_{CN}	0.086	1.908	0.4917
C_{CH_3}	0.1094	1.908	-0.5503
H_{CH_3}	0.0157	1.487	0.1904
O_{H_2O}	0.1521	1.7682	-0.834
H_{H_2O}	0.046	0.2245	0.417
Bond	**k_b (kcal mol^{-1} Å^{-2})**	**r_{min} (Å)**	
C_{CN}–N_{CN}	600	1.157	
C_{CN}–C_{CH_3}	400	1.458	
C_{CH_3}–H_{CH_3}	340	1.09	
O_{H_2O}–H_{H_2O}	450	0.9572	
Angle	**k_θ (kcal mol^{-1} rad^{-2})**	**θ_{min} (Å)**	
N_{CN}–C_{CN}–C_{CH_3}	80	180.0	
C_{CN}–C_{CH_3}–H_{CH_3}	35	110.0	
H_{CH_3}–C_{CH_3}–H_{CH_3}	35	109.5	
H_{H_2O}–O_{H_2O}–H_{H_2O}	55	104.52	

The six-site (all-atom) acetonitrile potential model of Nikitin and Lyubartsev was chosen,[37] while TIP3P[38] was used for water, with all bonds to hydrogen kept rigid using the SHAKE algorithm.[39] Lennard-Jones, bonding and angle potential parameters used for acetonitrile and water in this study have been listed in Table 3.2. Compatibility of the two models was verified through comparison of bulk solution densities with those reported in literature,[27, 1, 40] and is presented in Figure 3.1.

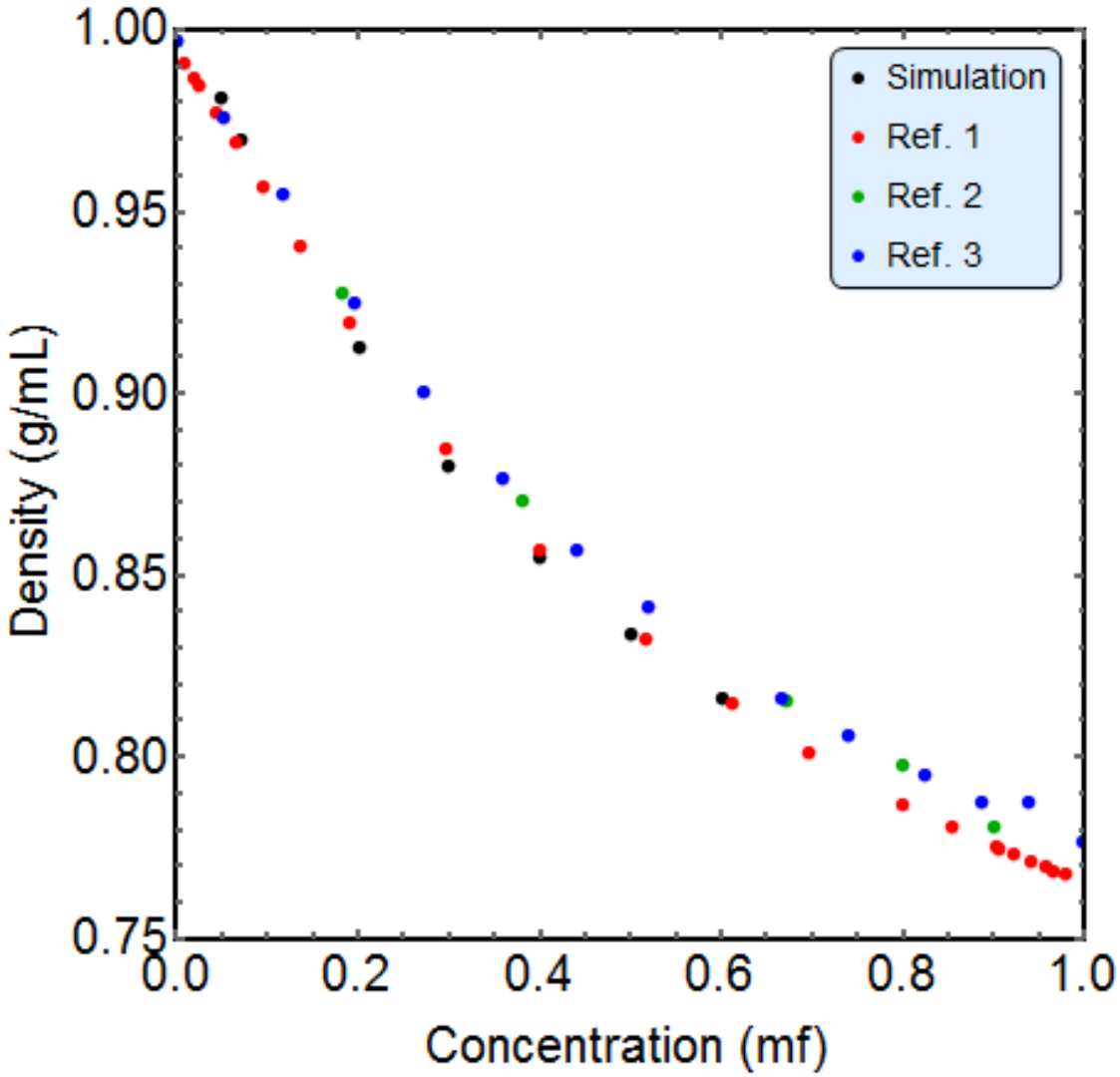

Figure 3.1: Solution bulk density as calculated from simulation (black), compared to experimental measurements of French[27] (red), Cunningham *et al.*[1] (green), and Grande and Marschoff[40] (blue).

Chapter 4

Results and Discussion

Bulk concentrations of aqueous MeCN between 0.032–0.59 mf have been investigated with correlations drawn between bulk and interfacial environments, primarily to expound the impact of short-range intermolecular structure on localized surface ordering. Effects on the latter from the former become evident as the surface population density begins to resemble that of the bulk. To illustrate this, we profile structural ordering in the surface and bulk environments independently, and highlight comparable features.

Consider first the depth-dependent density distribution of MeCN in aqueous solution. In the density profiles of Figure 4.1, is evidence of the preferential surface occupation of acetonitrile in dilute solutions. Here, profiles of MeCN and water are normalized to their respective bulk density. Through all compositions, the water density falls monotonically when approaching the vapor phase. Microheterogeneity however, is observed in the onset of inhomogeneous bulk water density beginning at 0.27 mf, in agreement with previous reports.[41, 42] Conversely, MeCN exhibits a measurable accumulation at the interface. This is especially true in dilute solutions. As the bulk concentration increases, surface enhancement is abated and the acetonitrile profiles become uniform throughout the slab.

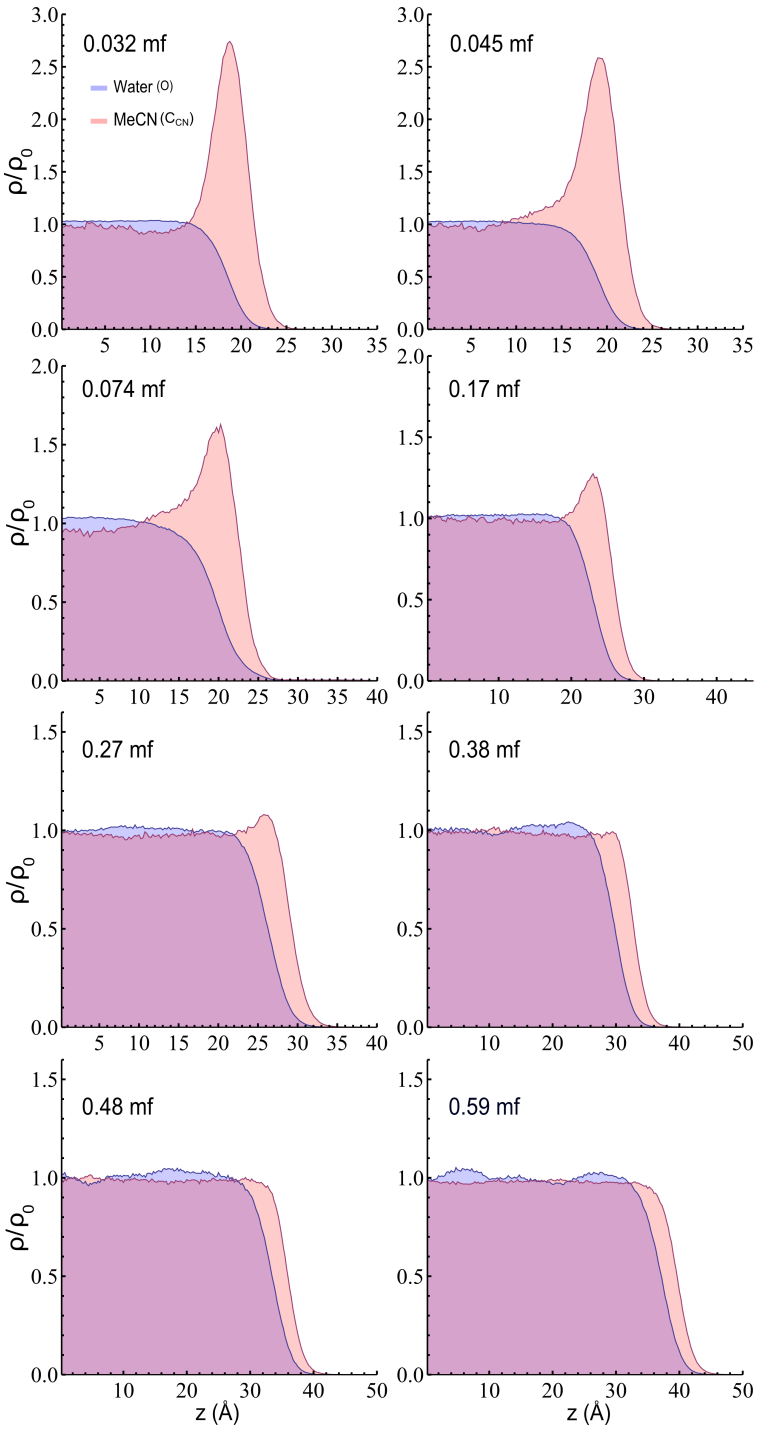

Figure 4.1: Density profiles for various concentrations of MeCN (red) in water (blue), following the methyl carbon and oxygen, respectively. The density ρ, normalized to the bulk density ρ_0, is histogrammed from the center of the slab ($z = 0$), and past the liquid/vapor interface. Dilute solutions exhibit a surface enhancement of MeCN, while the water density reduces monotonically toward the vapor phase.

Acetonitrile is also more highly exposed to vapor, as it is present beyond the extent of water at the solution surface. This organic solute diffuses to the interface and becomes trapped after dehydration of the methyl group, resulting in a water deficiency at the topmost layer.

To draw comparisons between interfacial and bulk phenomena, we identify a finite volume surface region near the interface. By surveying the average orientation of the MeCN dipole moment relative to the surface normal and as a function of depth (Figure 4.2a), the surface region is defined as bounded by the inflection and the point of upper termination. We assign the termination point as the depth at which interfacial MeCN density is half that of the bulk (from Figure 4.1), providing an upper bound to the surface. Then, an inflection from bulk isotropy to $cos(\theta) > 0$, offers a distinct transition between interfacial and bulk-like environments, thereby setting the lower bound. For solutions of all observed concentrations, the height of this surface region, defined in this manner, is approximately 5 Å.

Figure 4.2b is a representative cartoon model of the orientation of non-interacting acetonitrile molecules at the interface of a dilute aqueous solution. Surface occupied MeCN lay nearly flat, but gradually incline as they near the interface, such that the methyl group is farther from the solution. Angular probability distributions of Figure 4.2c and 4.2d (histogrammed with bins of 0.08 width), further implies a reduction of order at the surface with increasing concentration, attributed to flattening distributions. While true with respect to the natural solution axes, this particular analysis does not reflect any intermolecular relationship, for which there may be additional ordering.

Our results are in partial agreement with select aspects of multiple reports, such as flat-laying molecules[23, 24] and a tendency to flatten further as MeCN surface density increases,[18, 21]. However, these results are not in support of a low concentration 40° off-normal MeCN surface orientation, nor of an abrupt shift at 0.07 mf.[18] It is also at odds with suggestions of perpendicular orientation.[21, 25]

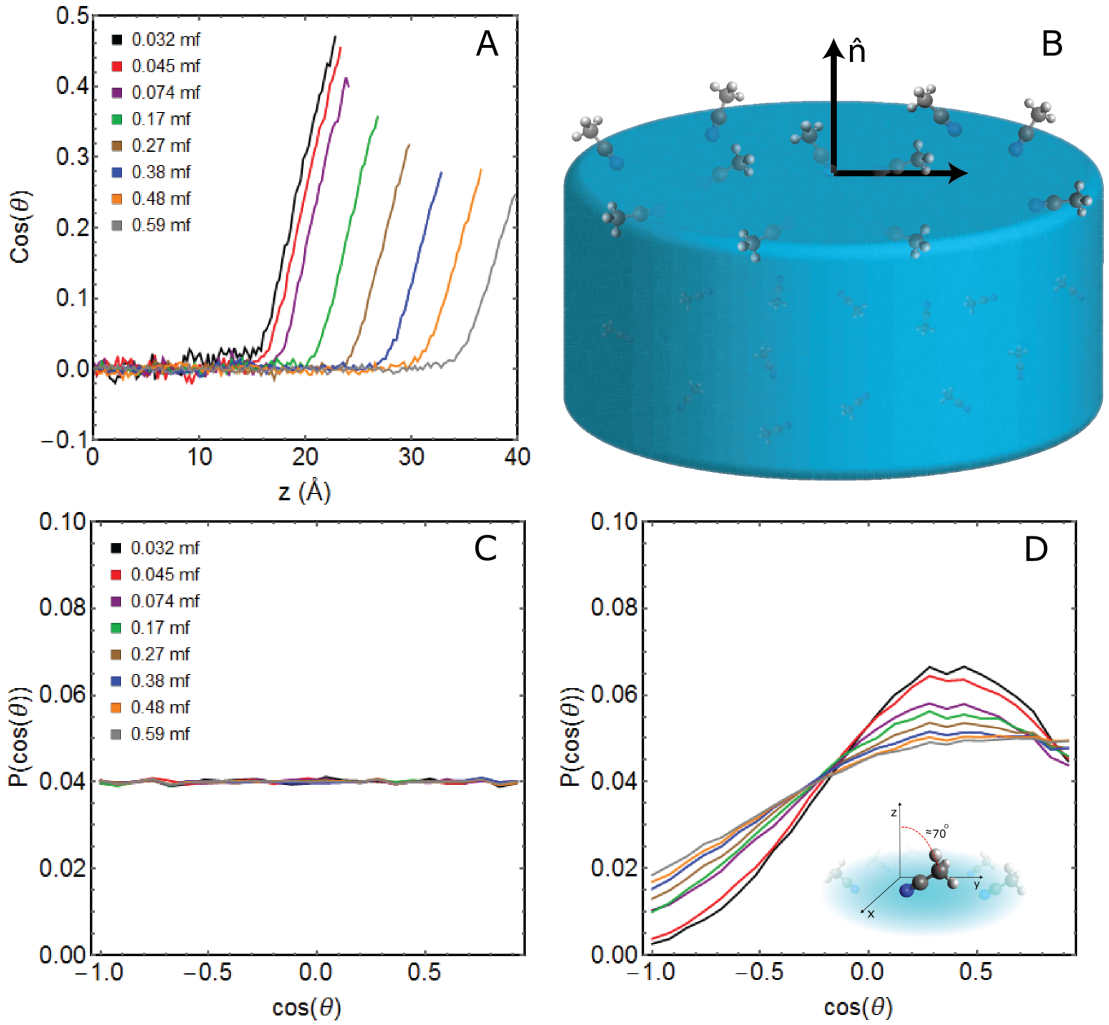

Figure 4.2: (a) Orientation of MeCN in solutions of varying concentration, with $z = 0$ as the center of the slab. Averaged angles are histogrammed over slab depth, with the center at $z = 0$. Angles are between the axes of the molecular dipole moment and the surface normal. (b) Cartoon model of the orientation of non-interacting surface-bound acetonitrile molecules. (c–d) Angular probability distribution of the MeCN in the bulk (c) and within the 5 Å surface region (d). The color scheme is common among all plots. Also, the inset of (d) demonstrates the surface distribution.

Now that we have a basic model of interfacial orientations in dilute solutions, what influence does a greater population density (i.e. molecules per unit volume) have on the angular distributions? In Figure 4.3a is such a comparison between that of the bulk and 5 Å surface regions. With bulk concentrations below 0.2 mf, the surface region has a larger MeCN population density, but is in fact less at higher concentrations. The reason for this is two-fold.

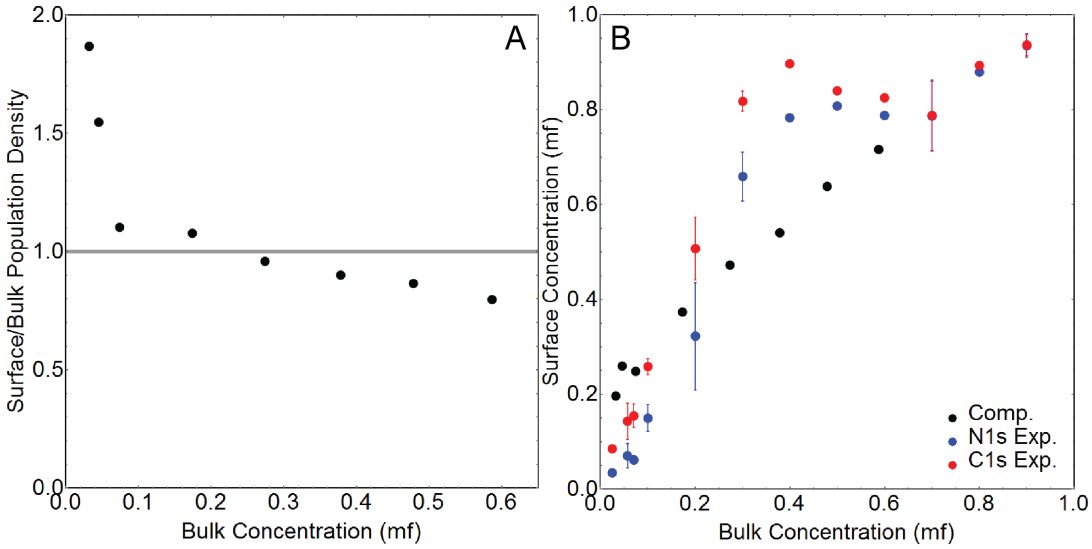

Figure 4.3: (a) Ratio of MeCN population densities ($\frac{molecules}{nm^3}$) in the bulk and 5 Å surface region over bulk MeCN concentration. (b) MeCN concentration computed from the top 5 Å surface region (black) compared to XPS concentration measurements using both N1s (blue) and C1s (red) photoemission signals at 200 eV kinetic energy.[26] Experimental data has been plotted with permission from the authors.

First, while the MeCN surface population continues to increase with total composition, it does so at a slower pace than in the bulk, due to the constraint of already possessing an energetically favorable orientation encouraged by dehydration of the methyl group. A larger population density at the surface, accompanied by a greater number of dipole-dipole interactions between neighboring MeCN, induces a slight change in the surface orientation, reducing the angle with respect to the surface plane. Second, along with the onset of microheterogeneity near 0.2–0.3 mf comes the formation of small aggregates of MeCN that

Table 4.1: Densities and orientations of MeCN in the 5 Å surface region

Bulk concentration (mf)	Average angle (deg.)	Bulk population density (nm^{-3})	Surface population density (nm^{-3})
0.032	72.9	1.10	2.06
0.045	73.9	1.61	2.49
0.074	75.6	2.44	2.69
0.17	78.9	4.42	4.77
0.27	80.7	6.06	5.81
0.38	81.8	7.38	6.66
0.48	82.1	8.37	7.24
0.59	83.1	9.27	7.40

inherently optimize their geometry by reducing the total occupied volume and, therefore, limit the number of interactions with water.

Surface and bulk population densities, as well as the average off-normal angle of MeCN in the 5 Å surface region have been listed in Table 4.1. Tabulated angles were computed from Figure 4.2a by averaging from the inflection to the upper termination point. A correlation between surface population density and angle is clear.

Like the population density, computed surface concentrations of MeCN ($\frac{No.of MeCN}{No.of MeCN+H_2O}$) are enhanced at low bulk concentrations (Figure 4.3b). The plotted experimental measurements are of ratios of 200 eV kinetic energy core orbital photoemission signals between acetonitrile C1s (or N1s) with the sum of C1s (or N1s) and water O1s.[26] The result is a surface sensitive concentration measurement. Although the general curve shape of the experimental and simulated results differ, both suggest surface concentration enhancement, although occurring at different bulk concentrations. Specifically, the computations convey a surface enhancement at bulk concentrations lesser than that implied by experiment. To note, simulation results presented here do not account for surface roughness. Instead, the liquid/vapor interface is defined by a macroscopic plane. Also, by treating the surface region as it is bounded by two planes, our definition of the surface differs from experiment, where one must rely on the

electron inelastic mean free path for interpreting the escape depth, and hence, the volume probed.

To further understand the impact of local interactions on surface structure, we compute a correlation function (Equation 4.1) relating in- and out-of-plane intermolecular spacing of MeCN, proposed by Tarek *et al.* and of the form:[43]

$$g_{NN}(s,z) = \sum_i \sum_j \frac{< N(s_{ij}, z_i, z_j) >}{\rho(z_j)\ 2\pi\ s\ ds\ dz} \delta(z - |z_i - z_j|). \tag{4.1}$$

This distribution function captures the average number of molecule pairs, $< N(s_{ij}, z_i, z_j) >$, of in-plane spacing (i.e. parallel to the macroscopic interfacial plane), $s_{ij} \pm ds$, of positions along the surface normal axis, $z_i \pm dz$ and $z_j \pm dz$, and normalized by the MeCN density, ρ at (z_j). A detailed derivation may be found in reference 43.

The distributions have been plotted as two dimensional contours for all concentrations in Figures 4.4–4.5, the former with the central MeCN molecule (N_i) originating in the bulk and the latter in the surface region. Here, z_{ij} is the intermolecular spacing along the surface normal, while s_{ij} has been defined above. The numeric scale (color scheme) of the contours differ slightly for each concentration, due to differences in the strength of the correlations, so the values for each have been listed in Tables 4.2–4.3.

The tables list the value for all ten contours of each plot. For example, in Table 4.2, the highest intensity contour (10) bounds correlations that are $>$ 0.0480 for an acetonitrile concentration of 0.032 mf. This corresponds to the highest intensity (red) contour for the plot of the same concentration in Figure 4.4. The lowest intensity contour (1) of Table 4.2; therefore, corresponds to the lowest intensity contour (light blue) of Figure 4.4. This also applies for interpreting Table 4.3 with respect to the correlations of Figure 4.5.

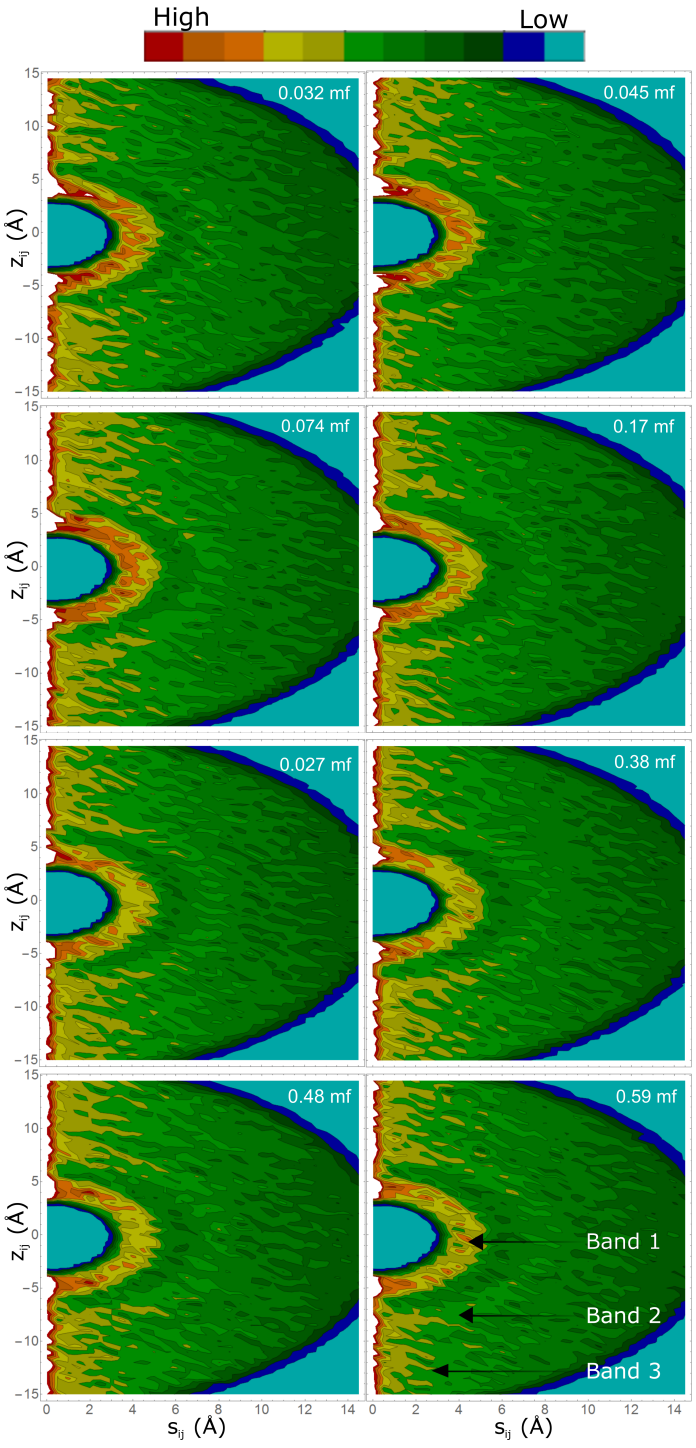

Figure 4.4: The correlation function of Equation 4.1 is plotted for MeCN of each simulated concentration with molecule N_i originating in bulk of solution. Intermolecular spacing along the surface normal and along a plane parallel to the surface are represented by z_{ij} and s_{ij}, respectively. Greater red intensity indicates a stronger correlation. Contour values are listed in Table 4.2.

Table 4.2: Numeric scale of contours (Con.) for distribution functions of Figure 4.4

Con.	0.032 mf	0.045 mf	0.074 mf	0.17 mf	0.27 mf	0.38 mf	0.48 mf	0.59 mf
10	0.0480	0.0990	0.230	0.870	1.70	2.50	3.20	4.00
9	0.0432	0.0891	0.207	0.783	1.53	2.25	2.88	3.60
8	0.0384	0.0792	0.184	0.696	1.36	2.00	2.56	3.20
7	0.0336	0.0693	0.161	0.609	1.19	1.75	2.24	2.80
6	0.0288	0.0594	0.138	0.522	1.02	1.50	1.92	2.40
5	0.0240	0.0495	0.115	0.435	0.85	1.25	1.60	2.00
4	0.0192	0.0396	0.092	0.348	0.68	1.00	1.28	1.60
3	0.0144	0.0297	0.069	0.261	0.51	0.75	0.96	1.20
2	0.0096	0.0198	0.046	0.174	0.34	0.50	0.64	0.80
1	0.0048	0.0099	0.023	0.087	0.17	0.25	0.32	0.40

Distribution functions for the central bulk molecules are plotted in Figure 4.4. Little to no data is registered within a 3 Å radius of the central molecule. Immediately beyond the first 3 Å is an enhanced correlation from near-neighbor pairing. This is followed by a dark band of lesser correlation, and then another bright band. At the highest of concentrations, these bands are slightly more evident and the correlation is greater (see Table 4.2 for contour values), given the larger number of MeCN molecules in solution and thus higher probability to interact. In fact, the first enhancement is nearly two orders of magnitude greater at 0.59 mf than at 0.032 mf.

Bands are indicative of local intermolecular order in the range of at least 10 Å, but likely as great as 15 Å. Despite weaker correlation at low concentrations, short range order persists. This may suggest a lesser form of microheterogeneity exists at lower concentrations than those reported.

As is expected within bulk solution, no preference for in-plane coordination is apparent, whereas broken symmetry at the liquid/vapor interface generates a different picture for the surface. In Figure 4.5, the band structure is similar. However, in-plane coordination prevails, given the preference for acetonitrile to remain at the interface and dehydrate the hydrophobic

Table 4.3: Numeric scale of contours (Con.) for distribution functions of Figure 4.5

Con.	0.032 mf	0.045 mf	0.074 mf	0.17 mf	0.27 mf	0.38 mf	0.48 mf	0.59 mf
10	0.0540	0.100	0.200	0.560	0.710	1.00	1.70	2.00
9	0.0486	0.090	0.180	0.504	0.639	0.90	1.53	1.80
8	0.0432	0.080	0.160	0.448	0.568	0.80	1.36	1.60
7	0.0378	0.070	0.140	0.392	0.497	0.70	1.19	1.40
6	0.0324	0.060	0.120	0.336	0.426	0.60	1.02	1.20
5	0.0270	0.050	0.100	0.280	0.355	0.50	0.85	1.00
4	0.0216	0.040	0.080	0.224	0.284	0.40	0.68	0.80
3	0.0162	0.030	0.060	0.168	0.213	0.30	0.51	0.60
2	0.0108	0.020	0.040	0.112	0.142	0.20	0.34	0.40
1	0.0054	0.010	0.020	0.056	0.071	0.10	0.17	0.20

methyl group. This is especially true for systems of low concentration. Upon a rise in population density, particularly at concentrations of 0.17 mf and above, the appearance of the distributions for surface incumbent molecules are very similar to those of the bulk.

Consulting Tables 4.2–4.3, one may observe, for 0.032–0.045 mf, a greater pair correlation for molecules at the surface; yet, in an equal mixture of water and MeCN, bulk pair correlations are double. As such, this reflects competition between rigid structural order at the interface and a high density induced intermolecular order. Differentiating MeCN surface and bulk structure then rests on understanding the impact of the imposed rotational restraints due to residing near the interface.

Presented in Figures 4.6–4.7 are series of probability distributions of the relative orientation between molecular dipoles, separated by r_{ij} (i.e. of molecules i and j). Plotted in each bin is the probability, $P(cos(\theta))$, which has been computed between $-1 < cos(\theta) < 1$, for many $r_{ij} \pm \Delta r$, with $\Delta r = 0.1$ Å. It is normalized such that individual columns sum to one. Simply, each column is an probability distribution of dipole-dipole relative orientations and has been plotted collectively as a two dimensional contour for convenient interpretation. Quantitative comparisons are justified only along isoradial bins.

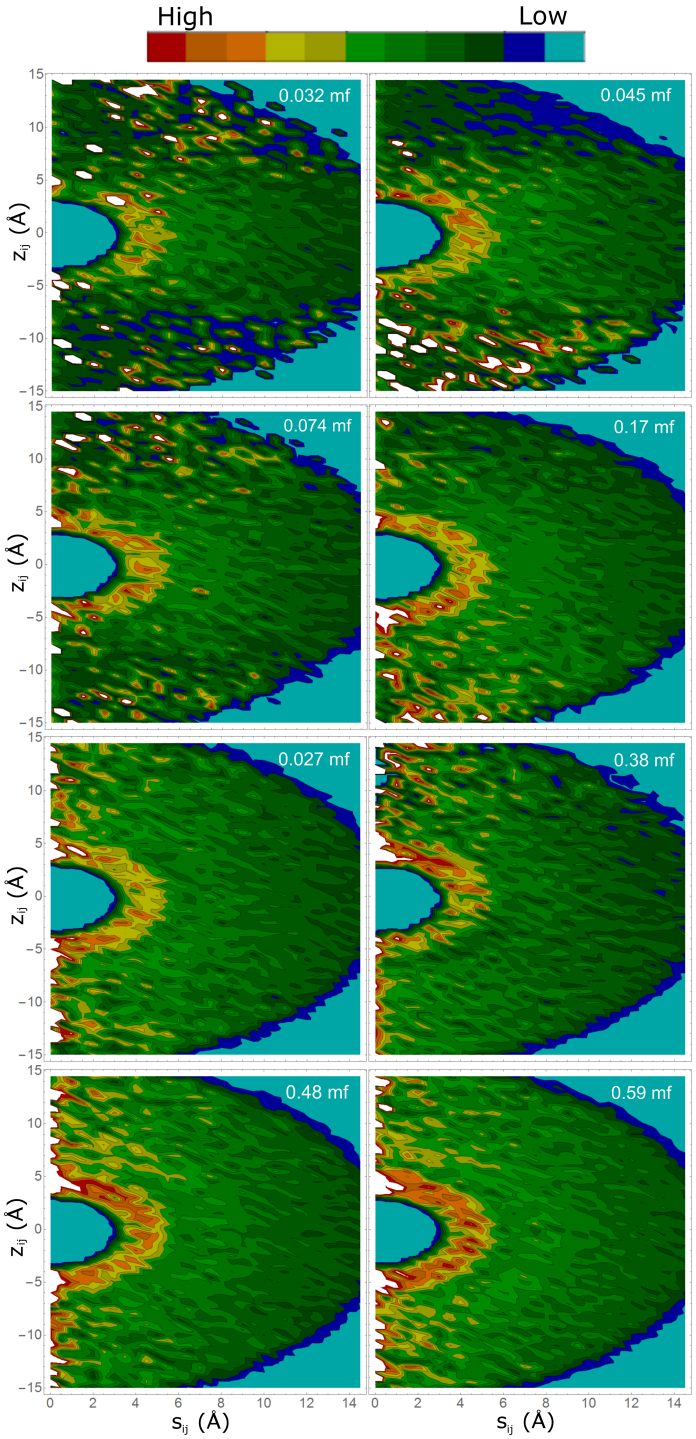

Figure 4.5: The correlation function of Equation 4.1 is plotted with molecule N_i originating in the surface region. Contour values are listed in Table 4.2.

Table 4.4: Numeric scale of contours for $P(cos(\theta))$ in Figures 4.6–4.7

Con.	0.032 mf	0.045–0.074 mf	0.17–0.38 mf	0.48–0.59 mf
7	0.0600 ± 0.0024	0.0575 ± 0.0035	0.0533 ± 0.0005	0.0540 ± 0.0018
6	0.0565	0.0550	0.0520	0.0525
5	0.0530	0.0525	0.0507	0.0510
4	0.0495	0.0500	0.0494	0.0495
3	0.0460	0.0475	0.0481	0.0480
2	0.0425	0.0450	0.0468	0.0465
1	0.0390	0.0425	0.0455	0.0450

The numeric scale corresponding to both surface and bulk related probability distributions has been listed in Table 4.4. Some contours, corresponding to multiple concentrations, share only marginally different definitions and thus have been assembled together. Consequently, listed errors specify the maximum variability in each of the contours across their respective concentrations. For example, between 0.17–0.38 mf, uncertainty in the precision of all contours is no worse than $P(cos(\theta)) = 0.0005$.

Now, in the bulk of solution (Figure 4.6), neighboring MeCN dipoles with 3–5 Å spacing will statistically favor antiparallel orientation, evidenced by the enhancement at $cos(\theta) = -1$. Indeed, the probability of finding $cos(\theta) < -0.5$ at this radial distance may be upwards of 35% more likely than any other possible configuration. Van der Waals forces appear to dominate local structure between paired acetonitrile in the bulk of solution, inevitably resulting in the onset of nonhomogeneous solvation in water. This structure essentially resembles a series of interleaved antiparallel molecules that may extend as far as 10 Å or greater at higher concentrations. Also, note that r_{ij} have been measured between the methyl centers of MeCN pairs, so any signals generated below $r_{ij} = 3$ Å are merely resultant of brief exposure to a neighboring methyl group during the course of the simulation. These occurrences, however, are minimized when near the interface and are not present in the plots of Figure 4.7.

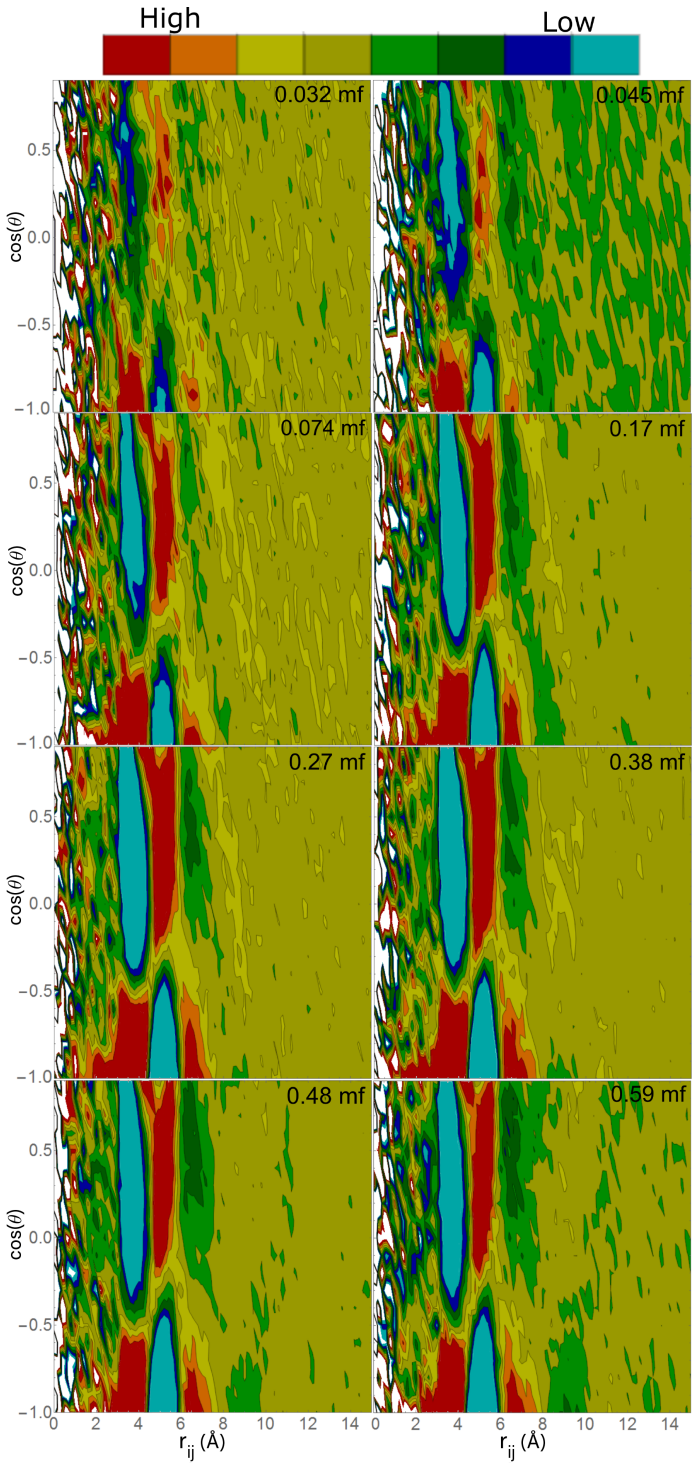

Figure 4.6: Probability distributions (of molecules in the bulk) for finding the relative orientation between two MeCN dipoles, $cos(\theta)$, is plotted for various values of intermolecular distance, $r_{ij} = R$. Each column (0.2 Å width) is individually normalized to one.

The probability distributions relating to surface-bound MeCN of Figure 4.7 share many of the same features as the bulk analogues. Arrangement of dipoles to form antiparallel pairs, as well as the extended structure at high concentrations is similar to bulk MeCN. Yet, at low concentrations this behavior is more pronounced at the surface than in the bulk. This is expected if one recalls both the greater in-plane correlation of Figure 4.5 and enhanced population density in the surface region present in Figure 4.3 for low concentrations.

Finally, antiparallel pairing of near-neighbor MeCN dipoles contributes to the flattening of the orientation of MeCN at the surface. Rather than subjecting acetonitrile to inversion at the interface, an increasing population density induces intermolecular order that permits the formation of nearly antiparallel pairs with the methyl groups slightly tilted above the interface. Ultimately, there is a measurable loss of order with respect to the macroscopic plane of the interface, but it is compensated through an enhanced intermolecular order.

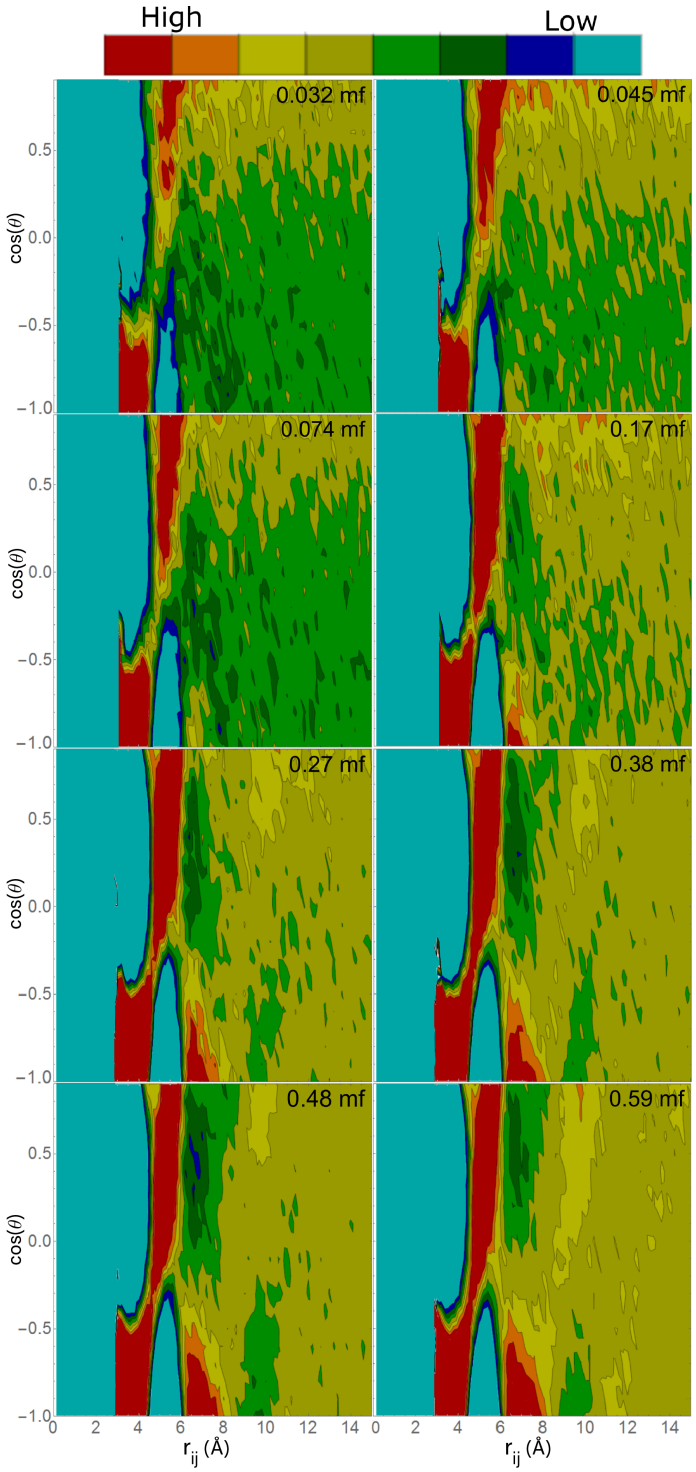

Figure 4.7: Probability distributions of the relative orientation between neighboring acetonitrile dipoles found in the surface region.

Chapter 5

Conclusion

Acetonitrile maintains an ordered structure at the liquid/vapor interface, encouraged by the hydrophobicity of MeCN and the affinity for the molecules to pair with immediate neighbors. Solutions of concentrations less than 0.2 mf experience a significantly enhanced adsorption of MeCN to the surface. The solute exhibits a preferential alignment of $> 70^{\circ}$ relative to the interface normal, but with increasing population density, an in-plane correlation is strengthened, antiparallel intermolecular layering persists and the prescribed interfacial order of non-interacting surface-bound acetonitrile flattens to nearly parallel.

Despite studying a deceivingly simple binary organic-water system, the competing interactions described here certainly provide an example of the complexity of chemistry at the liquid/vapor interface. I hope to have elucidated some of the previously unknown behaviors of acetonitrile at the aqueous solution interface, bridged existing gaps in the literature and encouraged further study of this and other similar systems with many shared questions yet to be answered satisfactorily.

Bibliography

[1] Cunningham, G. P.; Vidulich, G. A.; Kay, R. L. *J. Chem. Eng. Data* **1967**, *12*, 336–337.

[2] Arijs, E.; Brasseur, G. *J. Geophys. Res.* **1986**, *91*, 4003–4016.

[3] de Gouw, J. A.; Warneke, C.; Parish, D. D.; Holloway, J. S.; Trainer, M.; Fehsenfeld, F. C. *J. Geophys. Res.* **2003**, *108*, D11.

[4] Hamm, S.; Hahn, J.; Helas, G.; Warneck, P. *Geophys. Res. Lett.* **1984**, *11*, 1207–1210.

[5] Brasseur, G.; Arijs, E.; Rudder, A. D.; Nevejans, D.; Ingels, J. *Geophys. Res. Lett.* **1983**, *10*, 725–728.

[6] Kovacs, H.; Laaksonen, A. *J. Am. Chem. Soc.* **1991**, *113*, 5596–5605.

[7] Reimers, J. R.; Hall, L. E. *J. Am. Chem. Soc.* **1999**, *121*, 3730–3744.

[8] Bertie, J. E.; Lan, Z. *J. Phys. Chem. B* **1997**, *101*, 4111–4119.

[9] Jamroz, D.; Stangret, J.; Lindgren, J. *J. Am. Chem. Soc.* **1993**, *115*, 6165–6168.

[10] Venables, D. S.; Schmuttenmaer, C. A. *J. Chem. Phys.* **2000**, *113*, 11222–11236.

[11] Takamuku, T.; Noguchi, Y.; Matsugami, M.; Iwase, H.; Otomo, T.; Nagao, M. *J. Mol. Liq.* **2007**, *136*, 147–155.

[12] Takamuku, T.; Tabata, M.; Yamaguchi, A.; Nishimoto, J.; Kumamoto, M.; Wakita, H.; Yamaguchi, T. *J. Phys. Chem. B* **1998**, *102*, 8880–8888.

[13] Takamuku, T.; Noguchi, Y.; Nakano, M.; Matsugami, M.; Iwasi, H.; Otomo, T. *J. Ceram. Soc. Jpn.* **2007**, *115*, 861–866.

[14] Damewood Jr., J. R.; Kumpf, R. A. *J. Phys. Chem.* **1987**, *91*, 3449–3452.

[15] Dunn, W. J.; Nagy, P. J. *J. Chem. Phys.* **1990**, *94*, 2099–2105.

[16] Mountain, R. D. *J. Phys. Chem. A* **1999**, *103*, 10744–10748.

[17] Mountain, R. D. *J. Phys. Chem. B* **2010**, *114*, 16460–16464.

[18] Zhang, D.; Gutow, J. H.; Eisenthal, K. B. *J. Chem. Phys.* **1993**, *98*, 5099–5101.

[19] Zhang, D.; Gutow, J. H.; Eisenthal, K. B. *Faraday* **1996**, *92*, 539–543.

[20] Wang, H.; Borguet, E.; Yan, C. Y.; Zhang, D.; Gutow, J.; Eisenthal, K. B. *Langmuir* **1998**, *14*, 1472–1477.

[21] Kim, J.; Chou, K. C.; Somorjai, G. A. *J. Phys. Chem. B* **2003**, *107*, 1592–1596.

[22] Ding, F.; Hu, Z.; Zhong, Q.; Manfred, K.; Gattass, R. R.; Brindza, M. R.; Fourkas, J. T.; Walker, R. A.; Weeks, J. D. *J. Phys. Chem. C* **2010**, *114*, 17651–17659.

[23] Paul, S.; Chandra, A. *J. Chem. Phys.* **2005**, *123*, 184706:1–8.

[24] Mountain, R. D. *J. Phys. Chem. B* **2001**, *105*, 6556–6561.

[25] Pártay, L. B.; Jedlovszky, P.; Horvai, G. *J. Phys. Chem. C* **2009**, *113*, 18173–18183.

[26] Perrine, K. A.; Margarella, A. M.; van Spyk, M. H. C.; Winter, B.; Faubel, M.; Bluhm, H.; Hemminger, J. C. *J. Phys. Chem. C* **2014**, *118*, 29378–29388.

[27] French, H. T. *J. Chem. Thermodyn.* **1987**, *19*, 1155–1161.

[28] Tuckerman, M. E. *Statistical Mechanics: theory and molecular simulation*; Oxford University Press, USA, 2010.

[29] Swope, W. C.; Anderson, H. C.; Berens, P. H.; Wilson, K. R. *J. Chem. Phys.* **1982**, *76*, 637–649.

[30] Verlet, L. *Phys. Rev.* **1967**, *159*, 98–103.

[31] Brooks, B. R.; Brccoleri, R. E.; Olafson, B. D.; States, D. J.; Swaminathan, S.; Karplus, M. *J. Comput. Chem.* **1983**, *4*, 187–217.

[32] Jones, J. E. L.; Devonshire, A. F. *Proc. Roy. Soc. Lon.* **1939**, *169*, 317–338.

[33] Allen, M. P.; Tildesley, D. J. *Computer Simulation of Liquids*; Clarendon Press, 1989.

[34] Essmann, U.; Perera, L.; Berkowitz, M. L.; Darden, T.; Lee, H.; Pedersen, L. G. *J. Chem. Phys.* **1995**, *103*, 8577–8593.

[35] Phillips, J. C.; Braun, R.; Wang, W.; Gumbart, J.; Tajkhorshid, E.; Villa, E.; Chipot, C.; Skeel, R. D.; e, L. K.; Schulten, K. *J. Comp. Chem.* **2005**, *26*, 1781–1802.

[36] Humphrey, W.; Dalke, A.; Schulten, K. *J. Mol. Graphics* **1996**, *14*, 33–38.

[37] Nikitin, A. M.; Lyubartsev, A. P. *J. Comput. Chem.* **2007**, *28*, 2020–2026.

[38] Jorgensen, W. L.; Chandrasekhar, J.; Madura, J. D.; Impey, R. W.; Klein, M. L. *J. Chem. Phys* **1983**, *79(2)*, 926–935.

[39] Ryckaert, J.-P.; Ciccotti, G.; Berendsen, H. J. C. *J. Comput. Phys.* **1977**, *23*, 327–341.

[40] del C. Grande, M.; Bianchi, H. L.; Marschoff, C. M. *J. Argent. Chem. Soc.* **2004**, *92*, 109–114.

[41] Blandamer, M. J.; Blundell, N. J.; Burgess, J.; Cowles, H. J.; Horn, I. M. *J. Chem. Soc. Faraday Trans.* **1990**, *86*, 277–281.

[42] Marcus, Y.; Migron, Y. *J. Phys. Chem.* **1991**, *95*, 400–406.

[43] Tarek, M.; Tobias, D. J.; Klein, M. L. *J. Phys. Chem.* **1995**, *99*, 1393–1402.